Continental Shelf Research 205 (2020) 104195

Contents lists available at ScienceDirect

Continental Shelf Research

journal homepage: www.elsevier.com/locate/csr

Research papers

Tidal sand ridges on the shelf: A numerical study of their natural morphodynamic evolution and response to interventions

A. Nnafie *, T.B.J. Wolf, H.E. de Swart

Institute for Marine and Atmospheric research Utrecht (IMAU), Utrecht University, Princetonplein 5, 3584 CC Utrecht, The Netherlands

ARTICLE INFO

Keywords:
Tidal sand ridges
Continental shelf
Morphodynamic model
Delft3D
SWAN
Waves
Sand extraction
Artificial islands

ABSTRACT

Tidal sand ridges are large-scale bottom features that occur on continental shelves with strong tidal currents and abundance of sand. These ridges have longshore spacings of several kilometres, heights of tens of metres, they evolve on centennial time scales and their crests are cyclonically rotated with respect to the direction of the dominant tidal currents. The coupled Delft3D-SWAN numerical model is used to study the natural morphodynamic evolution of tidal sand ridges and their response to interventions (sand extraction and construction of islands) in a setting that resembles the Belgian shelf. New aspects in this study are that a sophisticated wave model (SWAN), a shelf with a sloping bottom and state-of-the-art formulations for sediment transport (including suspended load) are considered.

Starting from an initially flat bed, model results show that sand ridges develop on the shelf that have similar characteristics as those of observed tidal sand ridges. Results further show that ridges recover after sand extraction, i.e., the original sand volume of the ridge crests is recovered on decadal time scales. Deepening of the troughs provides sand for this recovery. The recovery of the ridges is weaker when pits are located further offshore and/or are deeper. Ridges recover faster when waves are included. If a sand pit is too deep (> 4 m), the ridge loses sand in the first tens of years prior to its recovery on longer time scales. This initial sand loss seems to agree with the observed loss of sand volume from a tidal sand ridge on the Belgium shelf (Kwinte Bank), which has been subject to intense extractions.

Model results further show that islands lose sand on decadal time scales until they eventually disappear. This sand loss is deposited on the crests and in the troughs. The presence of islands causes the surrounding ridges to break into smaller ridges that have smaller orientation angles than those of the natural case. Using different island configurations (location, geometry and number of islands, longshore distance between islands) does not lead to qualitative changes of the model results.

1. Introduction

On outer continental shelves, where sand is abundantly present and surface tidal current amplitudes are larger than about 0.5 m s^{-1}, a variety of different bottom features are observed. The focus of this study is on the largest of these features (horizontal length scales of several km, heights of tens of metres), which are called tidal sand ridges (Dyer and Huntley, 1999, and references therein). Their crests are generally 5°–30° cyclonically rotated (anticlockwise on the Northern Hemisphere) with respect to the dominant direction of tidal currents (Kenyon et al., 1981). The cross-sectional profiles of the ridges are asymmetrical, which indicates migration of these bedforms in the direction faced by their steeper side. Examples of continental shelves where tidal sand ridges are observed are those of the southern North Sea and East China Sea (Fig. 1), the Bay of Bengal (Off, 1963) and Florida (Davis et al., 1993). Tidal sand ridges provide diverse habitats for aquatic life (van Dijk et al., 2012; Atalah et al., 2013) and dissipate wave energy during storms (Spencer et al., 2015), and in doing so, they preserve the stability of the offshore ecological environment.

Tidal sand ridges are increasingly becoming subject to human interventions, such as the construction of offshore wind farms (Atalah et al., 2013) and extraction of sand (Van Lancker et al., 2010). Moreover, construction of offshore artificial islands in areas containing fields of tidal sand ridges is a new measure that is presently being considered in e.g. the Netherlands[1] and Belgium[2] to protect their coasts against the projected rapid rise in sea level by the end of this century. These interventions are expected to have a major impact on

* Corresponding author.
E-mail address: a.nnafie@uu.nl (A. Nnafie).
[1] http://www.springtij.nu/emergo/.
[2] http://www.kustvisie.be.

https://doi.org/10.1016/j.csr.2020.104195
Received 7 August 2019; Received in revised form 31 May 2020; Accepted 1 July 2020
Available online 3 July 2020

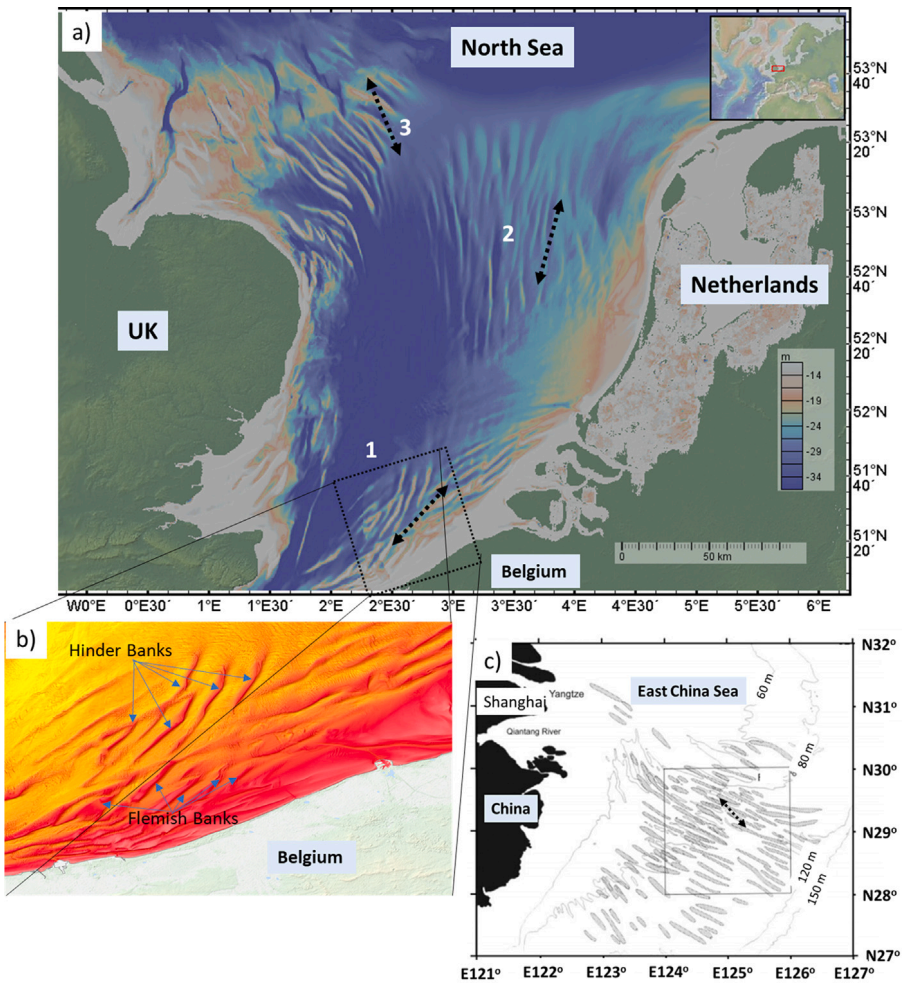

Fig. 1. (a) Bathymetric map of observed fields of tidal sand ridges in the southern North Sea. Numbers 1, 2 and 3 indicate respectively the Flemish/Hinder Banks, the Dutch Banks and the Norfolk Banks. A high resolution bathymetry of the Flemish/Hinder banks is displayed in panel b. (c) As in (a), but in the East China Sea. The dominant direction of flood and ebb flow is indicated by the black arrows. The map in panel a is obtained using GeoMapApp http://www.geomapapp.org;(Ryan et al., 2009) and the map in panel c is adapted from Liu et al. (2007). The zoom-in on the Flemish/Hinder banks (panel b) is generated by the EMODnet data portal (http://portal.emodnet-bathymetry.eu/).

the dynamics of the ridges. An example is the Kwinte Bank (part of Flemish Banks on the Belgian continental shelf, Fig. 1b), where a sand extraction pit continued to deepen and to broaden, resulting in the formation of a large depression area, even after cessation of extraction activities (Degrendele et al., 2010).

The formation of tidal sand ridges has been explained by means of the morphodynamic self-organization theory (Blondeaux, 2001; Dodd et al., 2003, and references therein). This theory states that small-amplitude bottom perturbations spontaneously grow in the case that they influence the flow in a way that sediment convergence takes place in the crest areas of these perturbations. It was first demonstrated by Huthnance (1982b), using linear stability analysis, that the formation of sand ridges could be explained by this theory. Later, full nonlinear approaches by Huthnance (1982a), Roos et al. (2004) and others (see review by de Swart and Yuan, 2018) were able to reproduce the gross characteristics (spatial pattern and height) of finite height sand ridges. Using a numerical model (Delft3D), Jiabi and Wang (2014) and Tao et al. (2019) successfully simulated the unique fan-shaped morphology of the radial sand ridges in the East China Sea. Yuan and de Swart (2017) revealed the influence of sea-level rise and related changes in tidal current on the long-term evolution of tidal sand ridges. van Veelen et al. (2018) were able to simulate the observed breaking of a single ridge into two or more ridges. However, the most previously cited models generally were limited by four rather strong assumptions: (1) highly simplified geometries were considered (flat bottom and dimensions in the order of several kilometres); (2) periodic boundary conditions of water level were used, which could not represent a propagating tidal wave correctly; (3) the parametrizations for waves did not account for wave directional spreading, refraction and wave-tide interaction; and (4) suspended sediment transport was neglected or modelled crudely.

Regarding the morphodynamic response of tidal sand ridges to sand extraction, Roos and Hulscher (2007) found that a ridge recovers on decadal time scales after a local removal of sand. The study by Roos et al. (2008) revealed that the presence of sand pits on a flat shelf bottom triggers a morphodynamic instability that causes formation of new tidal sand ridges. Brière et al. (2010), who modelled a 30 year morphodynamic evolution of the depression area that formed on top of the Kwinte Bank, did not find any recovery of this area during the modelling time period. However, these models are limited in the sense that they either addressed only the linear dynamics of perturbations induced by shallow pits on a flat shelf bottom (without the presence of tidal sand ridges), or simulation times were only a couple of decades, or they employed a 1D configuration (so the size of the sand pit is indefinite). Regarding offshore artificial islands, it is presently unknown what potential implications their presence will have for the morphodynamic evolution of tidal sand ridges.

The aims of the present work are threefold. The first is to study the natural morphodynamic evolution (i.e., in the absence of human interventions) of sand ridges in a more realistic setting. This means

that a propagating tidal wave, currents and waves and both bedload and suspended load transport on a shelf with a cross-shore slope and realistic dimensions will be considered. The second is to assess the morphodynamic response of sand ridges to sand extraction. In particular, the dependence of model results on the dredged amount of sand and the location of extraction will be addressed. Finally, the third is to quantify the impact of the presence of one or more islands on the evolution of the ridges. Different scenarios of island configuration (location, geometry and number of islands, longshore distance between islands) will be explored as well. To this end, the state-of-the-art coupled numerical morphodynamic model Delft3D-SWAN is used to simulate the currents, waves, sand transport and bed level evolution (Lesser et al., 2004). This model is applied in a depth-averaged mode (2DH).

A description of the model components, the model configuration, design of experiments and the methodology to analyse results is given in Section 2. Model results are presented in Section 3 and discussed in Section 4. Section 5 contains a summary and the conclusions.

2. Material and methods

2.1. Model description

The shelf is schematized as a rectangular domain (size: $L_x \times L_y$) (Fig. 2). A coordinate system is defined such that x and y are the cross-shore and alongshore coordinates, respectively, and z is the vertical coordinate. The model domain has an initially alongshore uniform and a sloping cross-shore depth $H(x)$, which varies linearly from H_0 at the transition to the nearshore zone to H_S at the seaward side. Bed level $z_b(x, y, t)$, which is defined with respect to mean sea level $z = 0$ (MSL), initially equals $z_b(x, y, 0) = -H(x)$. Bottom perturbations $h(x, y, t)$ are defined with respect to the initial bed level $z_b(x, y, 0)$, $D(x, y, t)$ is the total water depth: $D(x, y, t) = -z_b(x, y, t) + \zeta$, with ζ the free surface elevation with respect to MSL.

The Delft3D model consists of different modules, FLOW, WAVES, SED and MOR. The FLOW module used in this study solves the depth-averaged shallow water equations for currents. The waves are computed with SWAN, which is a third-generation wave model, which solves the spectral wave action balance (Booij et al., 1996). It includes advection of wave action per frequency by the group velocity, refraction of waves by topography and currents, nonlinear wave–wave interactions, source terms (due to wind) and sink terms (due to whitecapping, depth-induced wave breaking and bottom friction). In this study refraction of waves by topography and currents are accounted for, while the nonlinear interactions are neglected. Only swell waves are considered, i.e., no wave growth by wind. Dissipation due to whitecapping, depth-induced wave breaking and bottom friction are included, for which the formulations of, respectively, Komen and Hasselmann (1984), Battjes and Janssen (1978) and Hasselmann et al. (1973) are used. The sediment transport (module SED) is computed using the formulation of Van Rijn (1993), which accounts for bedload and suspended load transport under the action of both currents and waves. Local bed-slope effects on the sediment transport are accounted for in both the direction of the local flow (longitudinal bed slope) and in the direction perpendicular to that (transverse bed slope), with bed slope coefficients α_{BS} and α_{BN}, respectively. The onshore directed sand transport due to wave asymmetry and the offshore directed transport due to e.g. Stokes return flow are not included in this model. It is assumed that the former transport is counteracted by the latter, such that their net contribution to the cross-shore transport vanishes. Bed level z_b (in module MOR) is dynamically updated as a result of the net exchange of sediment between the water column and the bed and of divergence in the bedload sediment transport. A summary of all the equations is given in Section S2 of the Supporting Information (SI).

Following the boundary concepts discussed by Roelvink and Walstra (2004), in the Delft3D FLOW module, water level ζ is imposed at the seaward boundary and Neumann conditions (longshore gradients in water level ζ) are prescribed at the lateral boundaries (south and north; Fig. 2). Furthermore, in the SED module, zero gradients in the sediment concentration are imposed normal to seaward and lateral boundaries (Deltares, 2019). At the shoreward boundary, it is assumed that there is no cross-shore transport of fluid between the shelf and the nearshore zone, meaning that the velocity component u vanishes at $x = L_x$. Consequently, there is no advective transport at this boundary, but there will be a cross-shore diffusive transport due to local bed slopes. As boundary conditions for the SWAN model, waves with a constant significant wave height H_s, peak period T_p and wave direction θ (with respect to the positive y-axis) are applied at the seaward boundary.

2.2. Study area

The natural morphodynamic evolution of the tidal sand ridges and their response to human interventions (extraction of sand and construction of islands) are studied on a domain that resembles the Belgian continental shelf, which is located in the Southern Bight of the North Sea (Fig. 1b). This shelf extends to a maximum of 84 km from the present-day coastline (65 km long), which is oriented southwest–northeast (De Clercq et al., 2016). A 50 km wide region of this shelf features the presence of a number of tidal sand ridges. The Belgian continental shelf is dominated by strong tidal currents, which reach values up to 0.75 m/s (Baeye et al., 2011). Storm-driven currents are also important in this area, whose values range between 0.1 and 0.4 m/s. The tide on the Belgian shelf is predominantly semi-diurnal (M_2). The dominant wave conditions in this area are from the southwest (Verwaest et al., 2011), with typical significant wave heights of about 1 m.

One reason for selecting the Belgian continental shelf as a study area is because of its large availability of observational data on tides, waves and bathymetry. Moreover, the Kwinte tidal sand ridge is located in this area, which has been subject to intensive sand extraction since the 1970s. Another reason is that constructing of artificial islands on this shelf is currently being considered.

2.3. Model setting

The model domain is chosen such that the coast is aligned south–north (Fig. 2). To minimize boundary effects, the domain length is chosen larger than that of the Belgian shelf ($L_y = 75$ km). The domain width is $L_x = 50$ km. Based on a longshore-averaging of the EMODnet bathymetry shown in Fig. 1b, the cross-shore bottom of the Belgian shelf is approximated by a linearly increasing depth from $H_0 = 5$ m at the shoreward side to $H_0 = 38.5$ m at the seaward side.

Based on observations (http://meetnetvlaamsebanken.be/), the model is forced by a northward propagating M_2 tidal wave with amplitude $\hat{\zeta}_2 = 1.8$ m and a phase difference $\Delta\phi_2 = 31.5°$ between southern and northern boundaries of the model domain. Furthermore, a 50-m thick bed layer is considered, which is assumed to consist of one single sand fraction with diameter $d_{50} = 200$ μm. This represents typical diameters of the sand grains of the Belgian shelf bed (Giardino et al., 2010). Based on field data, at the offshore boundaries in the SWAN model, waves are imposed that have a JONSWAP shape (with peak enhancement factor of 3.3 and directional spreading of 25°), a significant wave height of 1 m, peak wave period $T_p = 6$ s and wave direction $\theta = 220°$ (from the southwest).

The Delft3D and SWAN models solve the equations on rectilinear staggered grids, as depicted in Fig. 2b. Two computational domains are considered, i.e., a Delft3D (physical) domain (blue lines) with dimensions $L_x \times L_y = 50 \times 75$ km and a SWAN domain (blue and grey lines), which has much larger lateral and offshore extents than the former domain (dimensions 75 × 150 km). The use of a larger SWAN domain minimizes the formation of shadow zones (i.e., zones of strong reductions in wave height) at the southern boundary of the Delft3D domain. These zones are caused by the directional spreading

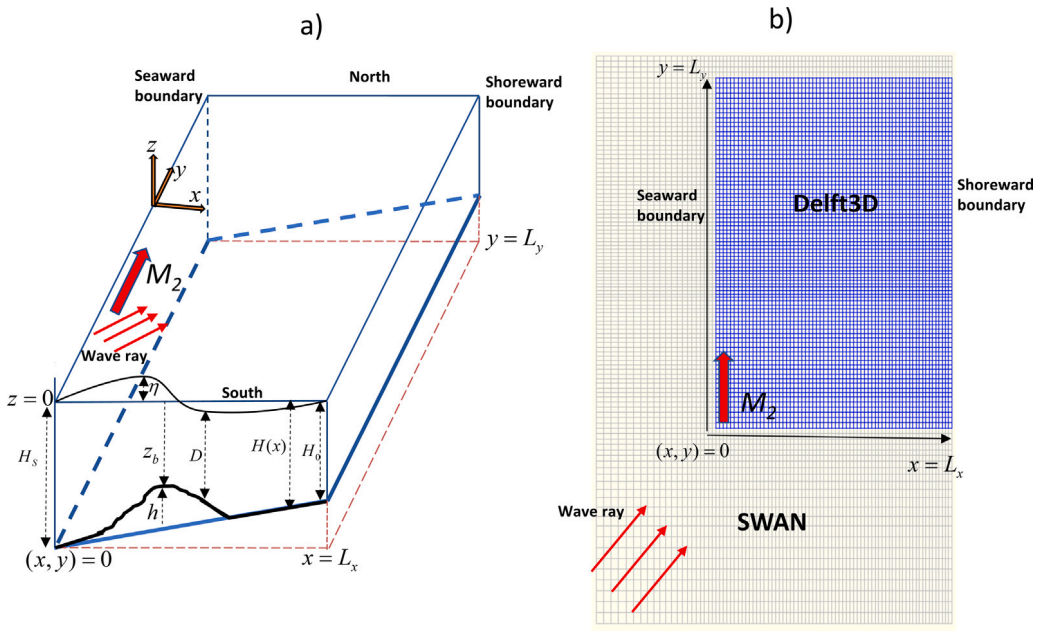

Fig. 2. (a) Schematic view of the rectangular shelf domain, with dimensions $L_x \times L_y$ and an initially alongshore uniform (y-direction) and cross-shore (x-direction) sloping bottom $H(x)$. A northward propagating semi-diurnal M_2 tidal wave and north-eastward propagating waves are imposed at the seaward boundary. For an explanation of other symbols, see the text. (b) Computational grids of SWAN (grey and blue) and Delft3D (blue), where the latter grid is nested in the former grid. (For interpretation of the references to colour in this figure legend, the reader is referred to the web version of this article.)

of waves, particularly in the case of imposing obliquely incident waves at the seaward boundary, as is the case in the present study. Grid cells of the blue computational grid have sizes of about 800 m, while those of the grey grid have a variable size that increases from ~800 m in the study area to ~2000 m at the seaward boundary.

Since the morphodynamic timescale is much longer (order of years) than the hydrodynamic timescale (order of days), a morphological acceleration factor $\alpha_{MOR} = 200$ is used to reduce computation time (Roelvink, 2006). Using lower values for α_{MOR} (= 25, 50, 100) does not yield different results. To further reduce computation times, the time interval of the communication between Delft3D and SWAN is set to 60 min (see Section S2.5 of SI). In the SWAN model, the directional space covers the full circle and is decomposed into 36 bins. The frequency space (consisting of 24 bins) is distributed between $f = 0.1$ Hz and $f = 0.25$ Hz. An overview of all model parameters is presented in Table 1.

Table 1
Overview model parameters.

Parameter	Value	Description
Physical domain		
L_x	50 km	Width of domain
L_y	75 km	Length of domain
H_S	38.5 m	Depth at seaward boundary
H_0	5.0 m	Depth at shoreward boundary
Flow		
f	1.43×10^{-4} s^{-1}	Coriolis parameter
C	65 m$^{1/2}$ s^{-1}	Chézy coefficient
ν	1 m^{2}s^{-1}	Horizontal eddy viscosity
$\hat{\zeta}_{2S}$, $\hat{\zeta}_{2N}$	1.8 m, 1.8 m	M_2 amplitudes at south/north boundaries
$\hat{\phi}_{2S}$, $\hat{\phi}_{2N}$	0°, 31.5°	M_2 phases at south/north boundaries
ω	1.405×10^{-4} s^{-1}	M_2 angular frequency
Wave		
θ	220°	Wave angle with respect to north
H_s	1 m	Significant wave height
T_p	6 s	Peak wave period
DR	25°	Directional spreading
Sediment		
d_{50}	200 μm	Diameter grain size
α_{BS}	1	Longitudinal bed slope coefficient
α_{BN}	20	Transverse bed slope coefficient
p	0.4	Bed porosity
Numerics		
Δt	60 s	Time step
α_{mor}	200	Morphological acceleration factor
Grid size	~800 m	Size grid cells
Directional bins	36	Number of directional bins in SWAN
Frequency bins	24	Number of frequency bins in SWAN
Frequency interval	[0.1–0.25] Hz	Lowest and highest frequency in SWAN

2.4. Natural morphodynamic evolution

The natural morphodynamic evolution of the tidal sand ridges (first objective) is addressed by running the model from the initially alongshore uniform and cross-shore sloping bottom $z_b = -H(x)$, to which small random bottom perturbation h with an amplitude of 2 cm are added (run 'SpinUp' in Table 2). Preliminary results show that a simulation time period of 500 years is sufficient for mature sand ridges to develop on the shelf. The duration of this simulation is 1000 years.

The simulated pattern of sand ridges after 500 years of morphodynamic evolution acts as a starting time (t_s) to address the morphodynamic response of these bedforms to human interventions. A larger starting time (t_s = 800 yr) will be considered as well (Runs 'Sandpit-SensTime' and 'Island-SensTime' in Table 2). The focus is on the response of the shelf to interventions on time scales that are relevant for coastal engineering purposes, i.e., maximal 200 years.

2.5. Sand extraction

The morphodynamic response of the ridges to sand extraction (second objective) is studied by creating a pit on the crest of a ridge at a distance $d_p = 5$ km from the shoreward boundary (run 'SandpitDefault'). The sand pit has horizontal dimensions $s_x \times s_y = 1940 \times 1940$ m and a dredging depth $l_z = 1$ m below the actual bed level z_b (Fig. 3a–b). These values represent typical dimensions of sand pits that have been created on sand ridges of the Belgian continental shelf (Brière

Table 2
List of model runs. The dredged volumes represent the sand volumes removed from the crests. In the case that a pit is too deep ($l_z > 4$ m), part of the dredged sand comes from the trough (about 10 Mm^3 for $l_z = 8$ m).

Run names	Description
SpinUp	Natural morphodynamic evolution (no intervention).
SandpitDefault	Default sand pit: depth $l_z = 1$ m, location $d_p = 5$ km, dredged: ~4 Mm^3.
Sandpit-SensTime	Sand pit created at $t = 800$ yr, dredged: ~4 Mm^3.
Sandpit-Sensdp	Sand pit at distances $d_p = 10, 15, 20$ km, dredged: ~4 Mm^3.
Sandpit-Senslz	Sand pit with depths $l_z = [2, 4, 8]$ m, dredged: ~[8, 18, 25] Mm^3.
IslandDefault	Default island: $\hat{h}_i = 5$ m, $d_i = 10$ km, $i_x \times i_y = 5 \times 10$ km, dumped: ~940 Mm^3.
Island-SensTime	Island created at $t = 800$ yr, dumped: ~840 Mm^3.
Island-SensTo-di	Island at distances $d_i = [3, 25, 35]$ km, dumped: ~[710, 1370, 1700] Mm^3.
Island-SensTo-iy	Island with longshore sizes $i_y = [5, 15, 20]$ km, dumped: ~[470, 1370, 1800] Mm^3.
Island-Multiple	2 and 3 islands: inlet width = 5 km, $d_i = 10$ km, dumped: ~[1800, 2700] Mm^3.
2Islands-SensTo-InletWidth	2 islands with inlet width = 0, 5, 10, 15 km, dumped: ~1800 Mm^3.

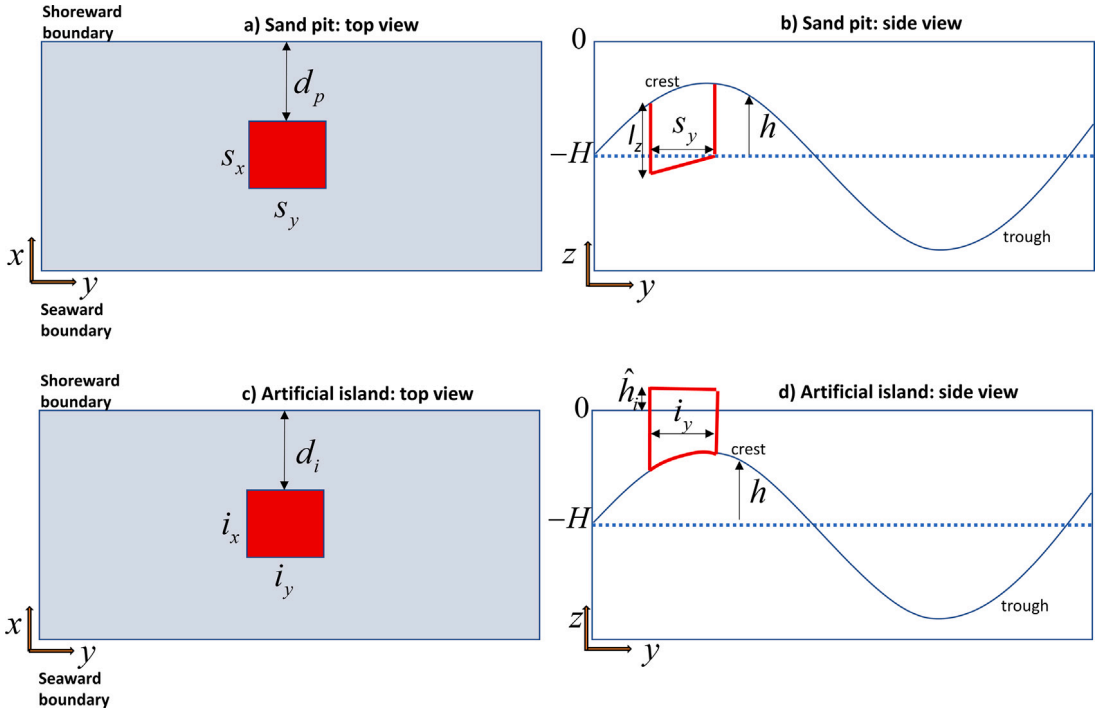

Fig. 3. Top and side views (red colours) of the extraction pit (a and b, respectively) and of the artificial island (c and d, respectively). The pit has dimensions $s_x \times s_y$, a cut depth l_z below bed level z_b and is located at a distance d_p from the shoreward boundary. The island is constructed at a distance d_i from the shoreward boundary, it has dimensions $i_x \times i_y$ and it sticks out above the water at height $\hat{h}_i$ with respect to mean sea level ($z = 0$). Note that these panels are only sketches; they do not represent the simulated bed levels.

et al., 2010). The sensitivity of model results to the cross-shore location d_p of the pit, as well as to its dredging volume V_d, is investigated by, respectively, constructing a pit further offshore ($d_p = 10, 15$ km, 'Sandpit-Sensdp') and by increasing its depth l_z ($l_z = 2, 4, 8$ m, 'Sandpit-Senslz'). Other parameter values of the pit configuration are kept constant at their default values.

2.6. Artificial islands

The morphodynamic response of the ridges to the presence of one or more islands (third objective) is assessed by first dumping sand at a distance $d_i = 10$ km from the shoreward boundary (run 'IslandDefault'), such that one island is created with a constant height $\hat{h}_i = 5$ m above MSL and horizontal dimensions $i_x \times i_y = 5 \times 10$ km (Fig. 3c–d). The choice for this geometry is motivated by the preliminary designs of artificial islands in the Belgian coastal zone (De Maerschalck et al., 2017). The island is allowed to erode during its morphodynamic evolution. Additional runs are conducted to explore the sensitivity of model results to different island configurations. In the first series of runs, the island is constructed at increasing distances from the shoreward boundary ($d_i = 3,\ 25,\ 35$ km, 'Island-SensTo-di'). In the second series, the island has different alongshore lengths ($i_y = 5,\ 15,\ 20$ km, runs 'Island-SensTo-iy'). In the fourth series, two and three islands (adjacent in longshore direction and 5 km spaced apart) are placed at distances $d_i = 10$ km ('Island-Multiple'). Finally, in the fifth series, two islands are placed with different inlet widths (longshore spacings), ranging between 0 and 15 km ('2Islands-SensTo-InletWidth'). Note that a 0 km inlet width represents two attached islands. In the case of multiple islands, each island has the default geometry, i.e., $i_x \times i_y = 5 \times 10$ km.

2.7. Key indicators

The morphodynamic response to an intervention is quantified in terms of (1) changes in the sand volume balance of the shelf domain with respect to the natural case (no intervention); and (2) the area of morphodynamic influence AMI.

The sand volume balance of the shelf domain is carried out by analysing the relative changes (with respect to the natural case) of the

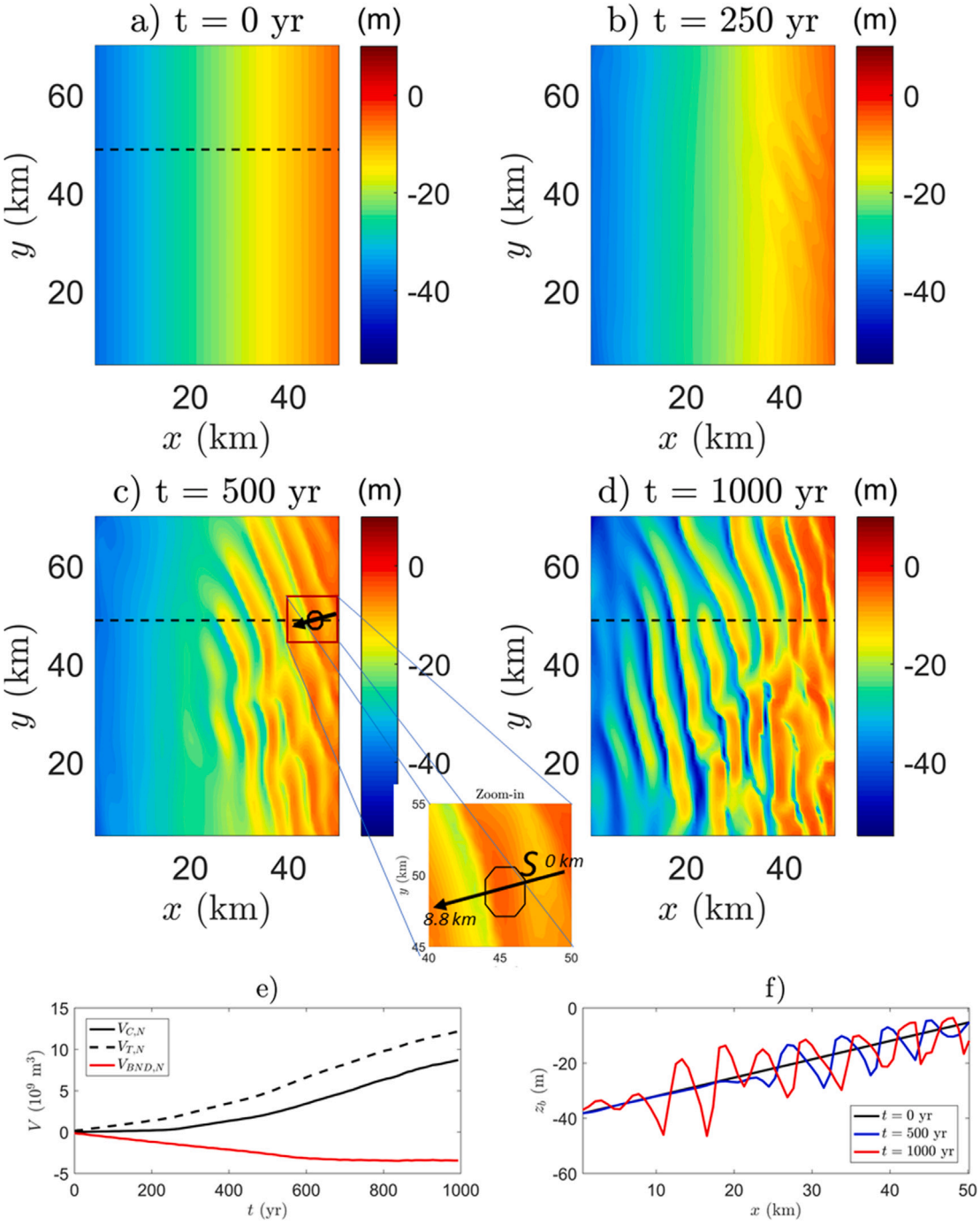

Fig. 4. Results from run 'SpinUp' (natural morphodynamic evolution). Snapshots of bed level z_b at times (a) $t = 0$ yr, (b) $t = 250$ yr, (c) $t = 500$ yr and (d) $t = 1000$ yr. Red and blue colours represent crests and troughs, respectively. The black circle and the arrow in panel c (see also the zoom-in) mark, respectively, the location of the sand pit used in the default extraction (run 'SandpitDefault' in Table 2) and a cross-crest transect S (with length 8.8 km) at this location. (e) Volume of crests $V_{C,N}$ (solid black line) and troughs $V_{T,N}$ (dashed black line) and the sand volume that is exchanged through the boundaries ($V_{BND,N}$, red line) versus time. (f) Bed level profiles along the cross-shore transects depicted in panels a, c and d (dashed black lines) at, respectively, times $t = 0$ yr (black), $t = 500$ yr (blue) and $t = 1000$ yr (red). (For interpretation of the references to colour in this figure legend, the reader is referred to the web version of this article.)

total volumes of all the crests and troughs of the bedforms of the shelf (V_C and V_T, respectively) and the relative changes of the sand volume that is lost or gained through the model boundaries (V_{BND}). Crest and trough volumes and the volume that is exchanged through the model boundaries are computed using

$$\begin{aligned} V_C(t) &= \iint_A h\ \Theta(h)\ dxdy, \\ V_T(t) &= \iint_A h\big(1-\Theta(h)\big)\ dxdy, \\ V_{BND}(t) &= V_C(t) - V_T(t) \quad \text{(sand volume balance).} \end{aligned} \tag{1}$$

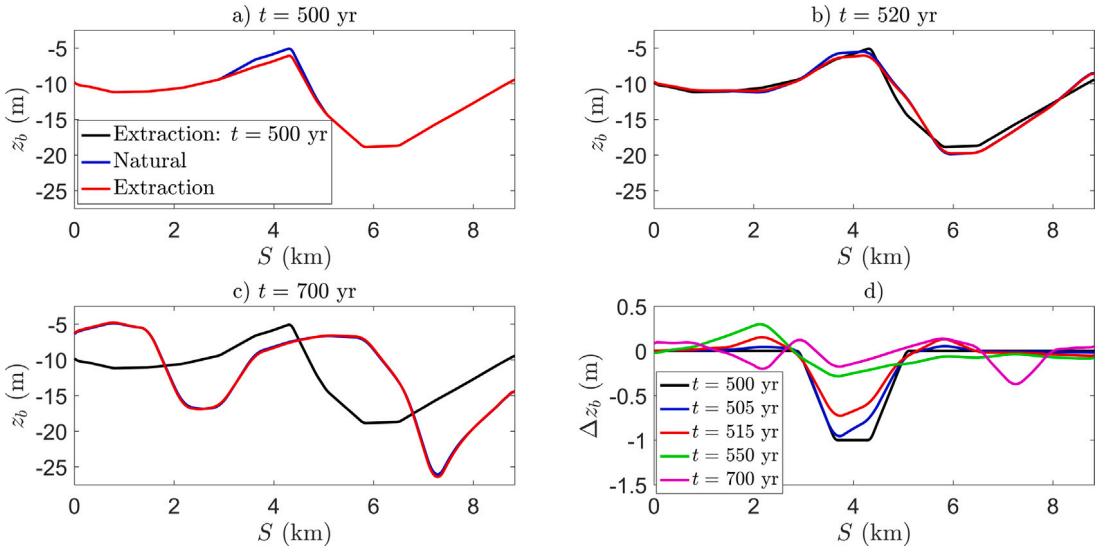

Fig. 5. Results from run 'SandpitDefault'. (a–e) Bed level profiles along the cross-crest transect S at the location of the pit in the cases with and without sand extraction (a–c) and their difference Δz_b (d) at different points in time between $t = 500$ yr and $t = 700$ yr. The locations of the pit and of the cross-crest transect S are shown in the zoom-in of Fig. 4c. Black lines represent the profile immediately after sand extraction ($t = 500$ yr). (For interpretation of the references to colour in this figure legend, the reader is referred to the web version of this article.)

Here, $\Theta(h)$ is a Heaviside step function with $\Theta(h) = 0$ for $h \leq 0$ and $\Theta(h) = 1$ for $h > 0$ and A is the surface area of the shelf. Furthermore, the following volume changes are defined:

$$\begin{aligned} \Delta V_C(t) &= V_{C,I}(t) - V_{C,N}(t), \\ \Delta V_T(t) &= V_{T,I}(t) - V_{T,N}(t), \\ \Delta V_{BND}(t) &= V_{BND,I}(t) - V_{BND,N}(t). \end{aligned} \tag{2}$$

In these expressions, $V_{C,I}$ and $V_{C,N}$ are the crest volumes in the case of an intervention (I) and in the natural case (N), respectively. Likewise, $V_{T,I}$ and $V_{T,N}$ are the trough volumes in the intervention case and natural case, and $V_{BND,I}$ and $V_{BND,N}$ are the exchange volumes for these two cases. A positive volume difference $\Delta V_C(t)$ means that, with respect to the natural case, crests undergo sand accumulation after the intervention, while negative values indicate erosion. In contrast, a positive volume difference ΔV_T indicates that, relative to the natural case, troughs experience sand erosion (deepening) and negative values represent accumulation (shallowing). A positive (negative) volume difference ΔV_{BND} reflects the situation where, in the case of an intervention, the shelf gains (loses) sand with respect to the natural case. For instance, if the shelf loses more (less) sand through the model boundaries in the case of an intervention compared with the natural case, this shelf experiences a sand loss (gain) after the intervention. In this study, ridges are said to fully recover after sand extraction if their total crest volume is equal to those of the natural case ($\Delta V_C = 0$). Sand that is used for this recovery might come from a deepening of the troughs (relative to the natural case, i.e., $\Delta V_T > 0$) and/or through the model boundaries ($\Delta V_{BND} > 0$).

In the case of an island, the difference between the volume of the island at a specific time, $V_{IS}(t)$, and the volume at the time of the intervention, $V_{IS}(t_s)$, is considered. This difference is denoted as $\Delta V_{IS}(t)$. The sand volume balance in the case of an island (relative to the natural case) reads

$$\Delta V_C(t) - \Delta V_T(t) + \Delta V_{IS}(t) + \Delta V_{BND}(t) = 0. \tag{3}$$

Following Roos et al. (2008), the area of morphodynamic influence AMI is defined as the surface area where the absolute differences between bed levels of the cases with and without intervention ($|\Delta z_b|$) exceed 1% of the mean (undisturbed) depth of the shelf ($H_{mean} \sim 21$ m). Mathematically, this is expressed as

$$AMI(t) = \iint_A \Theta(|\Delta z_b| - 0.01 H_{mean})\, dxdy. \tag{4}$$

3. Results

3.1. Natural morphodynamic evolution

The snapshots depicted in Fig. 4a–d show that the random bottom perturbations imposed on the initial bathymetry evolve on a centennial time scale into large-scale elongated bedforms on the shelf. These bedforms initially form close to the shoreward boundary and then extend to the offshore area. From Fig. 4e it appears that crest and trough volumes of the bedforms continue to increase after the simulation time period, which reflects the ongoing growth of new bedforms on the most offshore parts of the model domain. The volume of the troughs ($V_{T,N}$, dashed black line) is larger than that of the crests ($V_{C,N}$, solid black line), which reflects that not all the sediment that originates from the deepening of the troughs is deposited on the crest. Instead, a considerable amount of this sediment ($V_{BND,N}$, red line) is lost through the boundaries (after about 550 years at a constant rate of ~3 million m^3 per year). Fig. 4f shows that bedforms reach heights (crest-to-trough distances) up to 30 m in the nearshore area. They have lengths in the order of tens of kilometres, a wavelength of about 6 km and their crests are rotated cyclonically (with angles up to 30°) with respect to the main south–north direction of the tidal current. These bottom patterns resemble tidal sand ridges, which will be further discussed in Section 4.

3.2. Sand extraction

Default extraction.

In the case of the default sand extraction (run 'SandpitDefault'), an amount of $V_d \simeq 3.76$ million m^3 sand is extracted from the ridge crest at location $(x, y) = (45, 50)$ km (Fig. 4c). Snapshots of bed level profiles along the cross-crest transect at the location of the extraction of the cases with and without extraction (Fig. 5a–c; bed level profiles along the along-crest transect are shown in Fig. S1 in the SI) show that the disturbed ridge (red lines) tends to recover. Zooming in on the difference Δz_b between the two bed level profiles (Fig. 5d), it appears that besides infilling of the sand pit, the pit also widens in time. Moreover, alternating areas of erosion and sedimentation occur in the vicinity of the pit. From Fig. 6a–d, which displays the difference between bed levels of the cases with and without sand extraction (Δz_b) in the $x - y$ domain, it is seen that the sand pit (panel a) gradually deforms over time, with humps appearing around the pit (panel b).

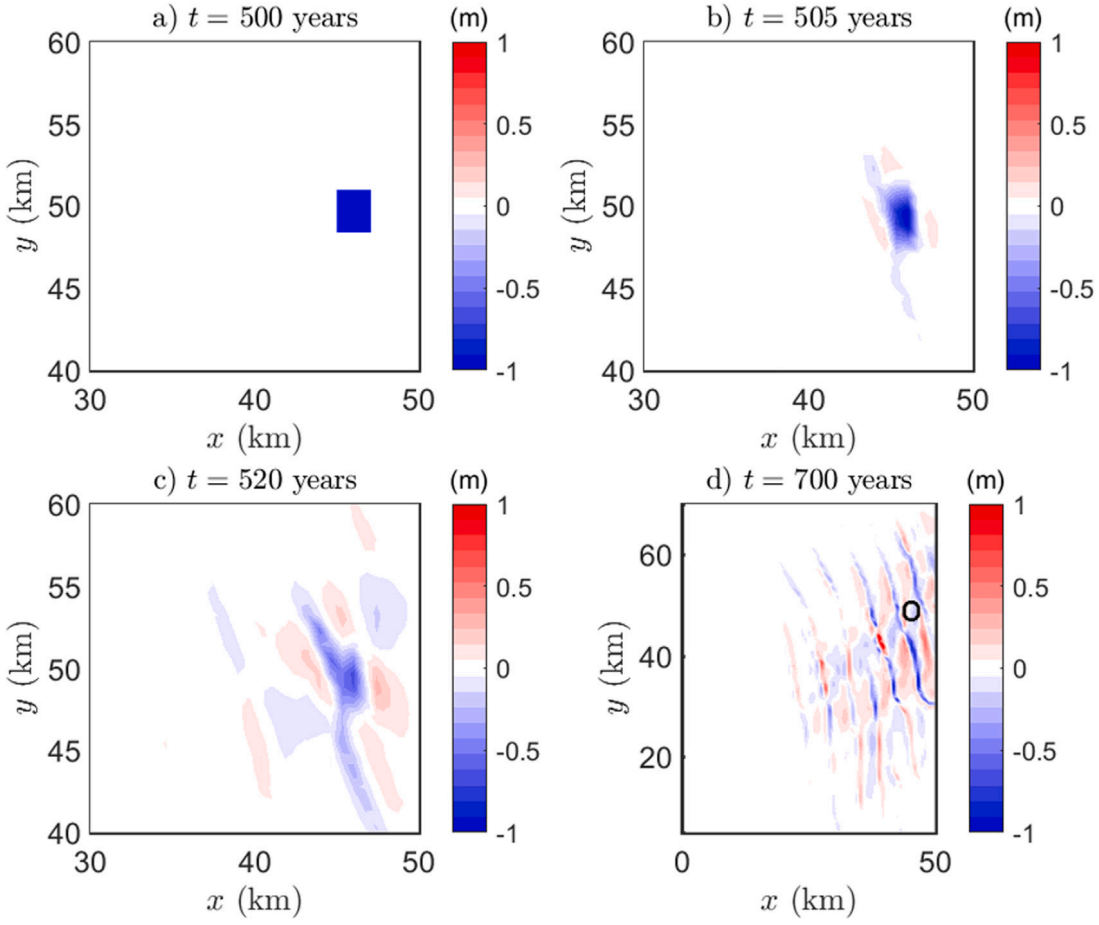

Fig. 6. Results from run 'SandpitDefault'. (a–d) Difference Δz_b between the bed levels of the cases with and without extraction in the x–y domain at different times after the intervention ($t = 500, 505, 520, 700$ years.). The black circle in panel d denotes the location of the sand pit.

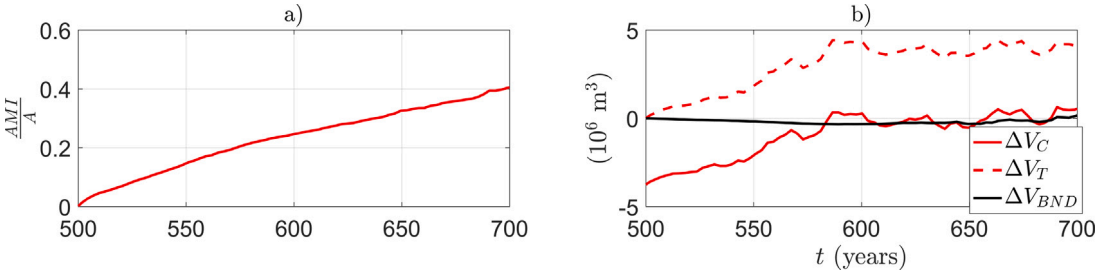

Fig. 7. Results from run 'SandpitDefault'. (a) Time evolution of the area of morphodynamic influence AMI (scaled by the total surface area A). (b) As in (a), but for the differences between the crest volumes (ΔV_C, solid red line), trough volumes (ΔV_T, red dashed line) and volumes that are exchanged through the boundaries (ΔV_{BND}, black line) of the cases with and without sand extraction. (For interpretation of the references to colour in this figure legend, the reader is referred to the web version of this article.)

Clearly, the presence of the sand pit triggers the formation of new bottom perturbations, which evolve into large-scale elongated and cyclonically oriented bedforms, resembling sand ridges (panels c–d). After 200 years of morphodynamic evolution, the area of morphodynamic influence AMI is about $0.4A$ (Fig. 7a), meaning that almost 40% of the total shelf area underwent bed level changes of at least 21 cm.

Analysis of the sand balance of the entire shelf (Fig. 7b) demonstrates that crests recover their natural volume ($\Delta V_C = 0$) within a time period t_r of ~87 years after sand extraction ($t \sim 587$ yr, red solid line). This recovery takes place at a rate of roughly 0.044 million m^3/yr. Eventually, after 200 yr of evolution ($t = 700$ yr), the total volume that is gained by the crests (relative to the natural case) is $\Delta V_C(t = 700\text{ yr}) - \Delta V_C(t = 500\text{ yr}) \sim 4.29$ million m^3. Thus, the crests not only have recovered the initial dredged amount ($V_d = -\Delta V_C(t = 500\text{ yr}) = 3.76$ million m^3), but their total crest volume at $t = 700$ yr is 0.53 million m^3 larger than that of the natural case. The increase in the volume of the troughs in the case of sand extraction with respect to the natural case (i.e., $\Delta V_T > 0$, red dashed line in Fig. 7b) indicates that troughs become deeper after sand extraction. About 94% of the total amount of sand that is made available through this deepening is used for the recovery of the crests, while 6% is lost through the model boundaries (at a rate of ~0.02 million m^3/yr). For $t > 685$ yr, the shelf starts to gain sand (at a rate of ~0.03 million m^3/yr). Note that sand losses and gains ΔV_{BND} (Fig. 7b) are computed relative to the natural case. Here, the initial sand loss caused by dredging ($= V_d$) is excluded.

Time of extraction, location and depth of the pit.

Extracting at a different time ($t = 800$ yr, run 'Sandpit-SensTime') does not qualitatively change model results (further details are given in

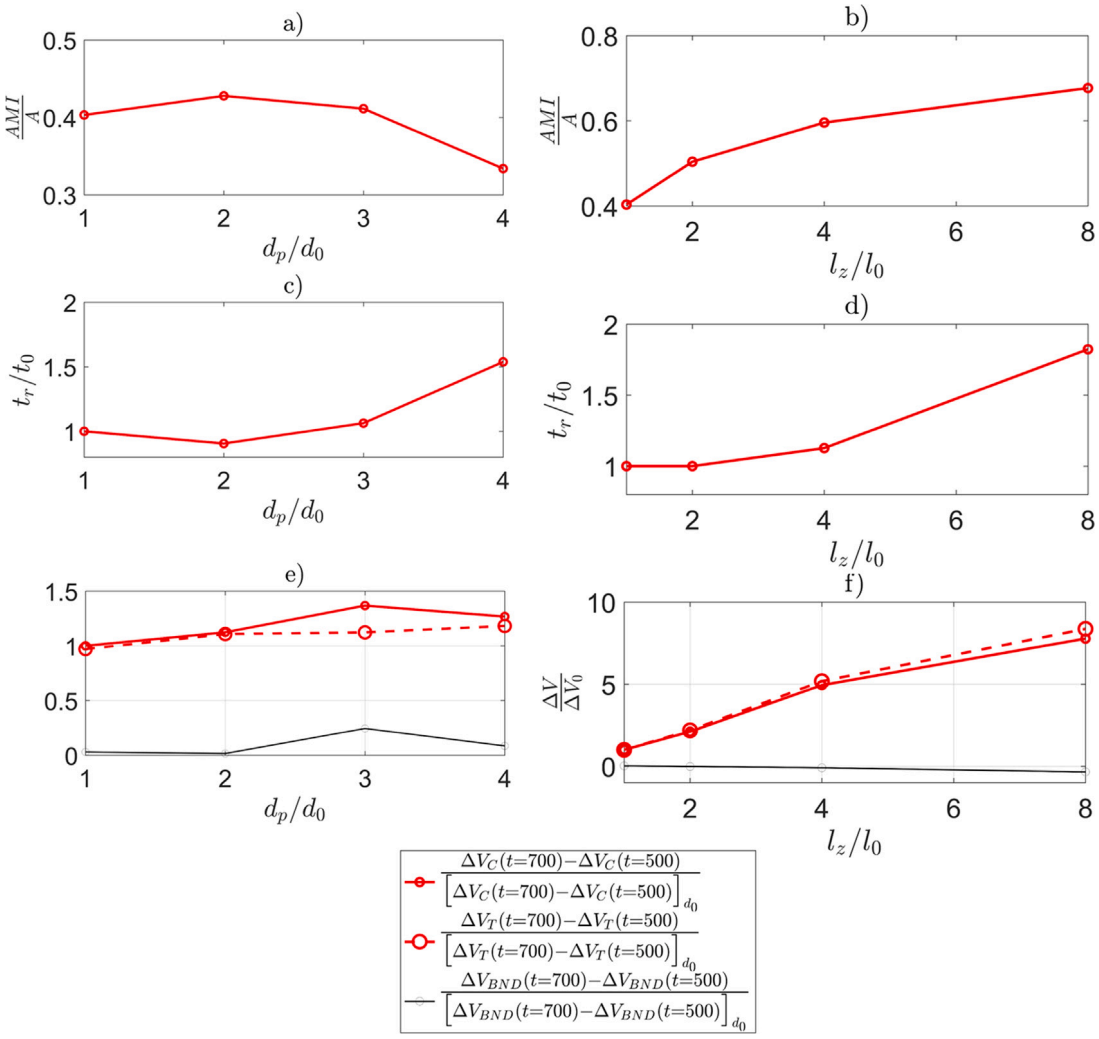

Fig. 8. Results from run series 'Sandpit-Sensdp' and 'Sandpit-Senslz'. Area of morphodynamic influence AMI (scaled by the total shelf area A) at $t = 700$ yr as a function of (a) distance d_p and (b) depth of the pit l_z. Distance d_p and depth l_z are scaled with their corresponding values of the default sand pit ($d_0 = 5$ km and $l_z = 1$ m). When changing distance d_p, the initial pit depth is kept constant at its default value (1 m) and when changing depth l_z, the pit location is held constant at its default value (5 km). (c–d) As in (a–b), but for the recovery time t_r of the ridge crest (scaled with its value in the case of the default sand extraction, $t_0 = 87$ yr). (e–f) As in (a–b), but for the volume differences between $t = 700$ yr and $t = 500$ yr of the crests ($\Delta V_C(t = 700\text{ yr}) - \Delta V_C(t = 500\text{ yr})$), troughs ($\Delta V_T(t = 700\text{ yr}) - \Delta V_T(t = 500)$) and of the sand exchange through the boundaries ($\Delta V_{BND}(t = 700\text{ yr}) - \Delta V_{BND}(t = 500\text{ yr})$). These volume differences are scaled with their corresponding values in the case of the default sand pit (Fig. 7b). (For interpretation of the references to colour in this figure legend, the reader is referred to the web version of this article.)

SI, Section S4). Model results for other locations (run series 'Sandpit-Sensdp') and larger volumes ('Sandpit-Senslz') of the sand pit reveal that the ridges respond to extraction in a similar way as in the case of the default sand pit. The main differences with respect to the default case are that the shelf area undergoes less bed level changes for far offshore located pits (18% less changes for $d_p = 20$ km, Fig. 8a) and more changes with increasing depth of the pit (about 3.6% more bed level changes per 1 m of increase in pit depth; panel b). Note that area AMI at first increases with increasing distance d_i, it reaches a maximum value (~$0.42A$) at $d_i = 10$ km, after which it decreases for larger d_i. Furthermore, compared with the default extraction case, it takes longer for ridges to recover in the case of a far offshore extraction (about 45 years longer for $d_p = 20$ km, panel c). A striking feature is that a ridge with a four times larger pit depth has a recovery time that is about 10 years longer than the ridge in the case of the default pit (panel d), suggesting that the recovery time is not proportional to the pit depth. Clearly, ridges recover at a faster rate in the case of larger pit depths (volumes). For instance, ridges recover at a rate of 0.16 million m^3/yr for $l_z/l_0 = 4$, which is 3.6 times larger than the recovery rate in the default sand extraction (0.044 million m^3/yr).

In almost all the cases of different locations and depths of the sand pit, the sand needed for the recovery of the crests comes from a deepening of the troughs (red lines in Fig. 8e). Exceptions are the far offshore located sand pits, particularly the pit that is located at $d_p = 15$ km ($d_p/d_0 = 3$), where approximately 17% of the total recovered sand is provided as a result of a smaller sand loss through the boundaries relative to the natural case (black line in Fig. 8e). Also in the case of larger depths of the sand pit, deepening of the troughs provides sand for the recovery of the ridge crests (Fig. 8f). In the case of large pit depths ($l_z/l_0 = 8$), about 4% of sand that comes from deepening of the troughs (dashed red line) is lost through the boundaries (black line). Results further demonstrate (Fig. S2 in SI) that in the case of a deep pit ($l_z = 8$ m), the crests lose sand in the first 50 years, after which they start to recover in the subsequent time period. The initial loss of sand is deposited in the troughs.

3.3. Artificial islands

Default island.

The presence of the default island (run 'IslandDefault') is established by depositing ~940 million m^3 sand at location $(x, y) = (40, 40)$ km at $t =$

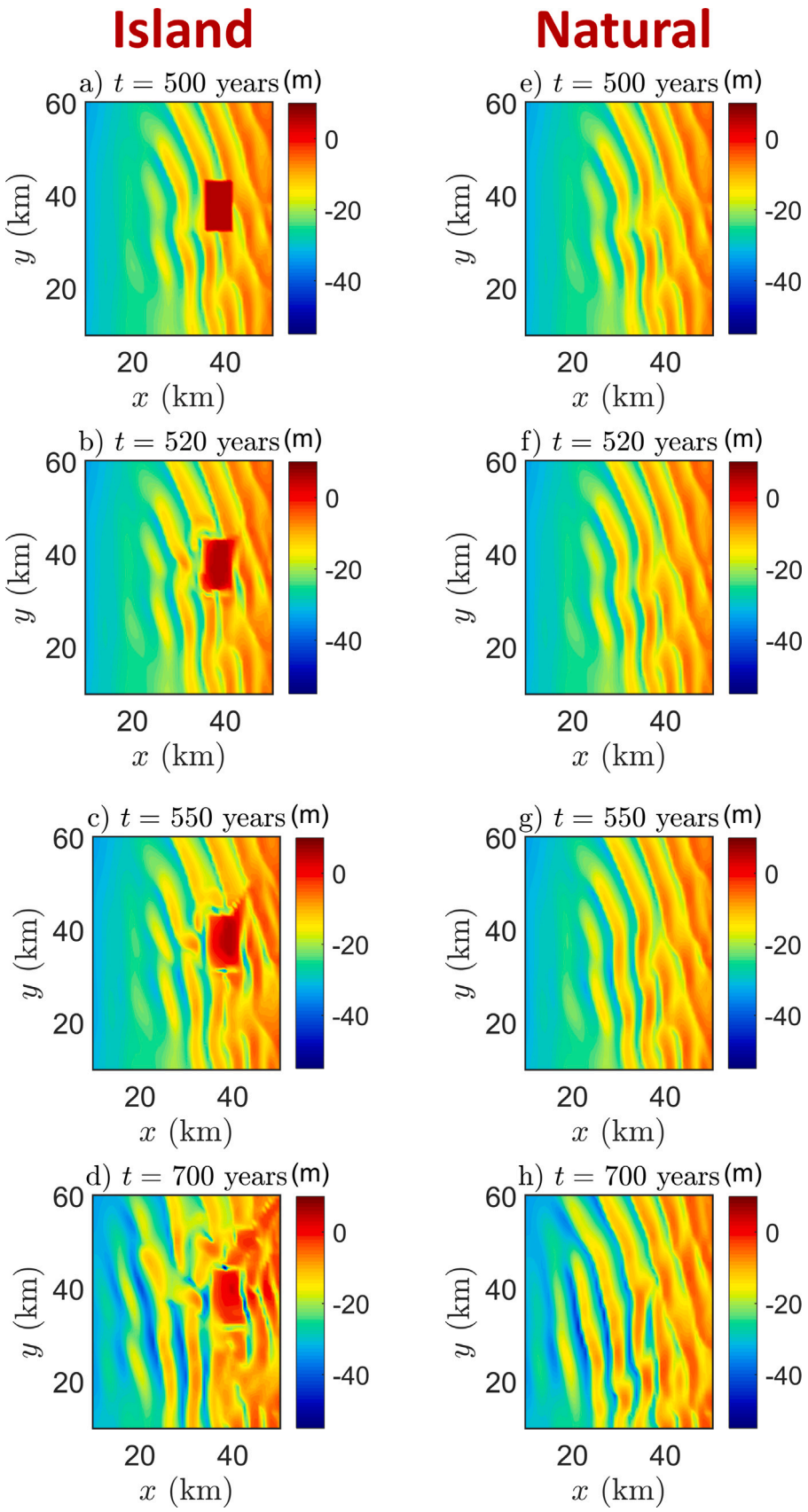

Fig. 9. Results from run 'IslandDefault'. Snapshots of bed level z_b between $t = 500$ yr (placement of island, run 'IslandDefault') and $t = 700$ yr in the cases with and without the default island (left and right panels, respectively).

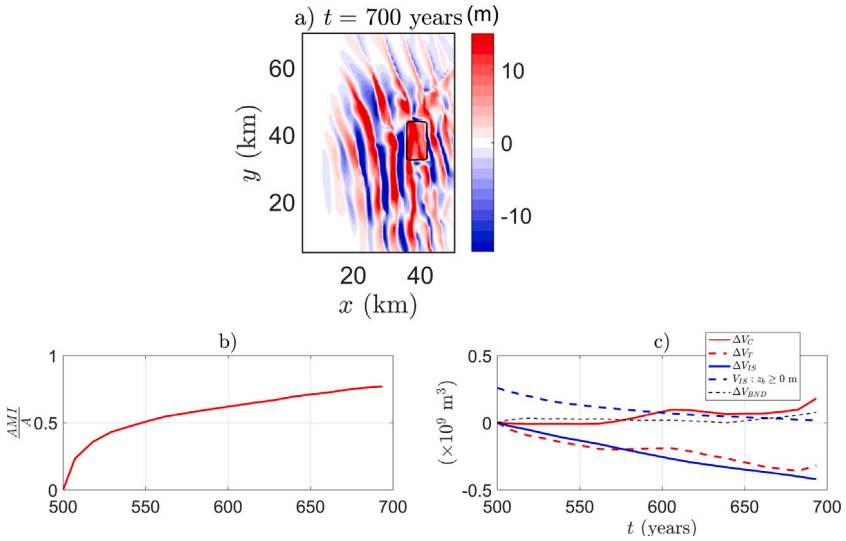

Fig. 10. (a) Difference between bed levels of the cases with and without the default island after 200 years of evolution ($t = 700$ yr). The black rectangle denotes the location of the island. (b) Time evolution of the (scaled) area of morphodynamic influence AMI (c) Sand balance of the shelf (relative to the natural case, Eq. (3)) versus time; ΔV_C and ΔV_T are differences between the crest and trough volumes of the cases with and without the default island and ΔV_{IS} is the total volume lost from the island (relative to its initial volume ($V_{IS}(t_s)$). Differences in the exchange volumes between the cases with an island and the natural case (ΔV_{BND}) are also shown. The volume of the part of the island that is located at or above MSL (V_{IS}, $z_b \geq 0$) versus time is also depicted. (For interpretation of the references to colour in this figure legend, the reader is referred to the web version of this article.)

500 yr (Fig. 9, panel a). This figure (panels b, c and d) demonstrates that the presence of an island strongly affects the alignment and longshore length of the surrounding sand ridges. Compared to the evolution of the ridges in the natural case (Fig. 9e–f-g–h), in the presence of the island, smaller scale ridges appear that have smaller angles with respect to the direction of the tidal current. Moreover, small-scale shoals and deep channels occur in the vicinity of the island (Fig. 9d). Similar to the cases of sand extraction, the presence of an island also triggers the formation of large-scale elongated and cyclonically oriented bottom perturbations that increasingly cover the shelf with time (Fig. 10, panel a). Almost the entire shelf undergoes bed level changes of at least 21 cm after 200 years of morphodynamic evolution (panel b).

From Fig. 10c it is seen that the island gradually loses sand over time, at an average rate of $\sim$ 2.5 million m^3/yr (solid blue line). As a result, part of the island that is located at or above MSL (dry island, $z_b \geq 0$) almost completely disappears after 200 years ($V_{IS} \sim 0$, dashed blue line). This sand loss from the island (ΔV_{IS}) is deposited on the crest and in the troughs (solid and dashed red lines), at rates of about 1 million m^3/yr and 1.5 million m^3/yr, respectively. Compared with the natural case, where the shelf loses sand through its boundaries (Section 3.1), this sand loss slightly reduces after placement of the island ($\Delta V_{BND} > 0$, dashed black line).

Different island configurations.

Similar to the case of sand extraction, constructing an island at a different time ($t_s = 800$ yr, run 'Island-SensTime') does not qualitatively change model results (Section S4). Results from sensitivity runs to the location of the island are presented in Fig. 11a–b, which shows the area of morphodynamic influence and the sand balance of the shelf (relative to the natural case) after 200 years of morphodynamic evolution. The area of morphodynamic influence is larger in the case of placing the island at more offshore locations compared with that in the case that the island is located closer to the shoreward boundary (panel a). Crests gain more sand with increasing offshore distance d_i (solid red line in panel b). Troughs are shallower (sedimentation) for an onshore located island ($d_i = 3, 10$ km) and they are deeper (erosion) for a far offshore located island ($d_i = 25, 35$ km, dashed red line in panel b). The sand loss from the island is stronger for an offshore located island (solid blue line), but the fact that this sand loss reduces for $d_i > 25$ km suggests that there exists an optimum in this loss ($\sim$ 3.26 million m^3/yr). The large sand gain by the crest in the case of a far offshore located island (about 6 million m^3/yr and 10 million m^3/yr for, respectively, $d_i = 25$ km and $d_i = 35$ km) is provided through the deepening of the troughs (dashed red line) and the sand loss from the island (solid blue line). In all the cases of different locations, the dry island ($z_b \geq 0$) eventually disappears after 200 years of evolution ($V_{IS} \sim 0$, dashed blue line). With respect to the natural case, the sand loss through the model boundaries reduces in all the cases of different island locations (solid black line).

The area of morphodynamic influence increases if the longshore size of the island (i_y) becomes larger (Fig. 11c). For all the cases with different island sizes ($i_y = 5, 10, 15, 20$ km), when compared with the natural case, both crests and troughs undergo sedimentation ($\Delta V_C > 0$ and $\Delta V_T < 0$), ranging between 1 and 3 million m^3/yr for each of them (panel d). This gain of sand is provided partly through sand loss from the island (in the range 1.6–2.5 million m^3/yr) and partly through a reduction in the sand loss through the boundaries (in the range 0.75–1.8 million m^3/yr). Apart from the case of the largest elongated island ($i_y = 20$ km), where the island still has a (dry) volume of about 70 million m^3 (above MSL) after 200 years of evolution, the (dry) island in all the other cases disappears in this period.

Results in the case of placement of more than one island do not qualitatively differ from those in the case that one island is present (Fig. 11e). Quantitative differences are that with increasing number of islands, more sand accumulates on the crests and in the troughs (an increase of about 1.7 million m^3/yr per added island, panel f, solid and dashed red lines). Sources for this sand accumulation are the sand loss from the island (solid blue line) and the reduction in the sand loss through the boundaries (relative to the natural case). All the (dry) islands have disappeared after 200 years of evolution.

Results from sensitivity runs to the longshore spacings between two islands (inlet width) are presented in Fig. 11g–h. The area of morphodynamic influence slightly decreases with increasing inlet width (panel g). For all the different inlet widths, sedimentation occurs on the crests and in the troughs (panel h), with sand that is provided through the sand loss from the island and reduction of the sand loss through the boundaries (relative to the natural case). Overall, crests undergo less sedimentation with increasing inlet width, ranging from about 3.2 million m^3/yr for a 0-inlet width (islands are attached) to 1.2 million m^3/yr for an inlet width of 15 km. Maximum accumulation of sand in

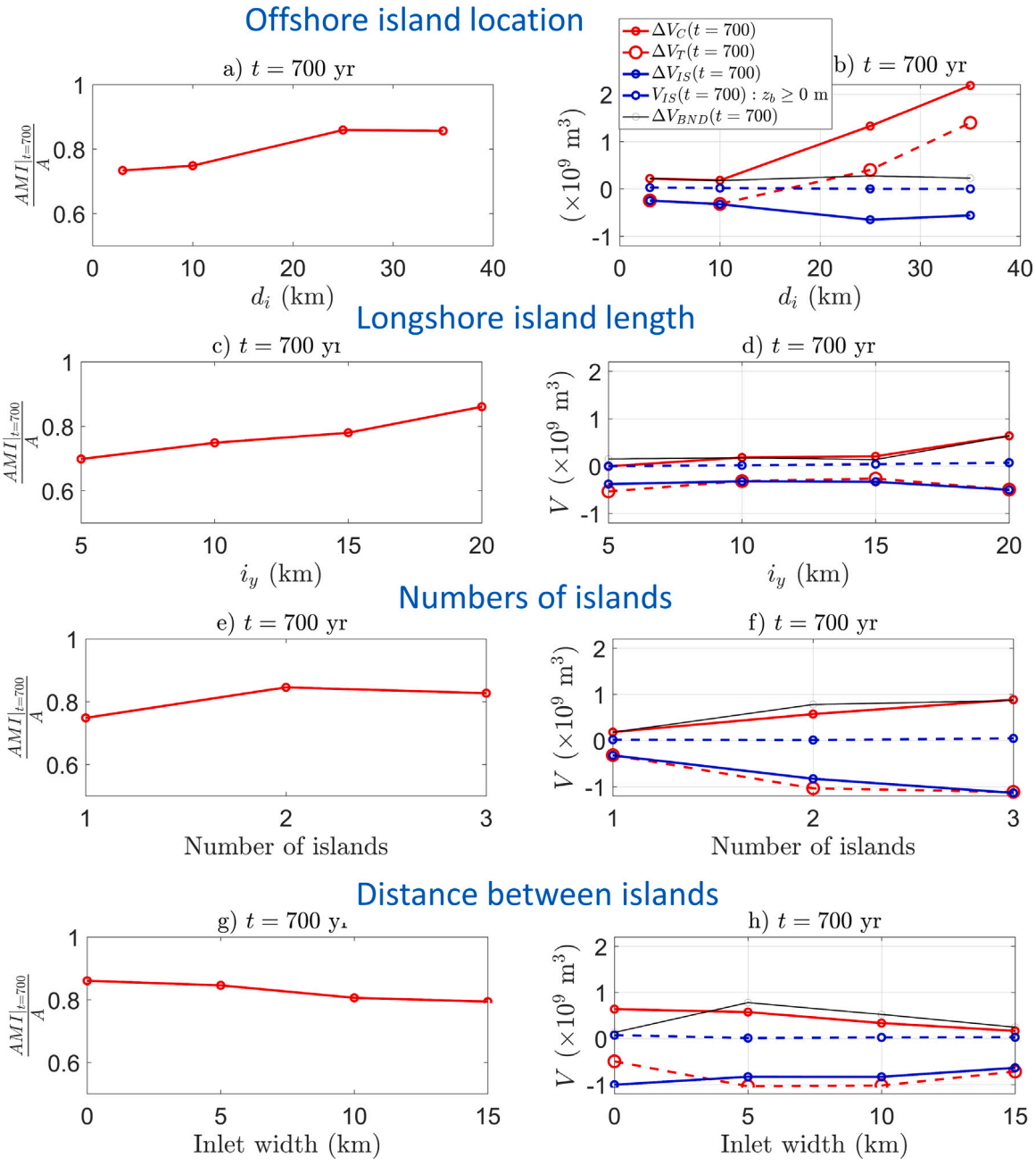

Fig. 11. Model results at $t = 700$ yr in the case of different island configurations (run series 'Island-SensTo-di', panels a–b; 'Island-SensTo-iy', panels c–d; 'Island-Multiple', panels e–f; and '2Islands-SensTo-InletWidth', panels g–h). Left panels: Area of morphodynamic influence AMI (scaled with shelf surface area A) at $t = 700$ yr as a function of the offshore location d_i (a) and longshore length of the island i_y (c), number of islands (e) and the inlet width between the islands (g). Right panels: As in the left panels, but for the volume differences at $t = 700$ yr of the crests ($\Delta V_C(t = 700$ yr)), troughs ($\Delta V_T(t = 700$ yr)) and of the sand exchange through the boundaries ($\Delta V_{BND}(t = 700$ yr)), the sand loss from the island ($\Delta V_{IS}(t = 700$ yr)) and the dry volume of the island ($V_{IS}(t = 700$ yr), $z_b \geq 0$). (For interpretation of the references to colour in this figure legend, the reader is referred to the web version of this article.)

the troughs (~3.2 million m^3/yr) appears for moderate inlets widths (5 and 10 km). In all the cases of different inlet widths, the (dry) islands completely disappear during the simulation time period.

4. Discussion

4.1. Natural morphodynamic evolution versus observations

The sand ridges obtained from the model in the case of their natural morphodynamic evolution (in the absence of interventions) are compared with the observed ridges on the Belgian continental shelf, viz. the Flemish banks and Hinder banks. The characteristics of the latter ridges are retrieved from the EMODnet bathymetric data shown in Fig. 1b (an overview of these characteristics is given in Table S2 of SI). The model simulates sand ridges with heights of up to 30 m, lengths and widths in the ranges 10–50 km and 2–4 km, respectively, a wavelength of about 6 km and crests that are rotated cyclonically at angles between 10° – 30° with respect to the direction of the tidal current (Fig. 4). These characteristics are in good agreement with those of the observed ridges. Moreover, a feature that appears during the model spin-up is the evolution of ridges into kinks (S-shape), which eventually break into two ridges (Fig. 4c–d). This feature might be the reason for the specific shape of some ridges on the Belgian shelf (i.e., Hinder banks, Fig. 1b) and on other shelves (e.g., Norfolk banks, Caston, 1972). According

to van Veelen et al. (2018), this feature arises when 1) the orientation of the ridge differs from its preferred orientation (according to linear theory) and 2) the ridge is sufficiently long for the crests to grow separately.

4.2. Sand extraction and artificial islands

Model results show that local bathymetric disturbances (Δz_b) on the shelf, either resulting from extraction of sand or dumping of sand in the case of islands, trigger the formation of new bottom perturbations, which evolve into large-scale elongated and cyclonically oriented bedforms that increasingly cover the shelf. Thus, introducing a local disturbance has a global impact on the shelf morphodynamic evolution. Note that the results of the sand extraction experiments extend those of Roos et al. (2008) to offshore sand pits of finite extent and depth of a shelf that is already covered by tidal sand ridges. Nevertheless, inspection of the difference plot of Fig. 12a, with superimposed the induced residual flow field, shows that the bottom perturbations induced by the pit behave quite similar as those in Roos et al. (2008). They interpreted their findings as that the joint action of friction and Coriolis forces causes the deformation and the elongation of the pit in the counterclockwise direction (Northern Hemisphere), as well as the appearance of adjacent humps. Patterns like those in Fig. 12b in the case of creation of an island can be understood from a similar reasoning.

These results mean that the presence of sand pits and artificial islands on a shelf with tidal sand ridges are morphodynamically unstable configurations. These islands will start to deform as a result of the tendency of the system to form cyclonically oriented bedforms. This deformation might be reduced by constructing elongated artificial islands along the crests of the ridges rather than parallel to the coast. Morphodynamically more stable islands might also be achieved by constructing them in areas where tidal sand ridges do not occur, such as the nearshore zone. Constructing of islands under these different conditions is a topic of future research.

4.3. Time scale of recovery from extraction

From model results it appears that ridges recover from sand extraction on time scales in the order of tens of years. The recovery time scale increases from $t_r \sim 90$ years for a 1 metre deep pit to $t_r \sim 160$ years for an 8 metre deep pit. It turns out that this time scale can be reasonably estimated by the following expression, which is based on the morphodynamic time scale that is derived by Roos et al. (2008) in their study of the morphodynamic evolution of offshore sand pits on a flat seabed:

$$t_r = \frac{(1-p)H_{mean}U_p}{\omega Q_p}. \tag{5}$$

Here, p is the porosity of the bed (= 0.4), H_{mean} is the mean (domain-averaged) depth of the shelf (~21 m), U_p and Q_p are the magnitudes of, respectively, the tidal current and suspended load transport (with unit of $m^3\ s^{-1}\ m^{-1}$) inside the extraction area. These magnitudes, which are presented in Table S1 of SI, are obtained from additional hydrodynamic experiments (flow over topography) for pit depths $l_z = 1, 2, 4, 8$ m. A comparison between the modelled and computed (using Eq. (5)) recovery time scales (Fig. 13(a)) indeed demonstrates that this equation is a reasonable estimation of the recovery time scales of the ridges, particularly for large pit depths ($l_z = 4, 8$ m). Note that the recovery time scale is rather sensitive to the magnitude of transport Q_p. The latter significantly increases during high waves and storms (increased stirring of sediment and higher currents), meaning that these conditions might speed up the recovery of the ridges from sand extraction. The role of waves in the recovery of ridges from sand extraction is also demonstrated by results from additional simulations, which are identical to those of 'SandpitDefault' and 'Sandpit-Senslz' ($l_z = 1, 8$ m) but without waves. These results (Fig. 13b–c) reveal that ridges recover more slowly when neglecting waves. This might explain why Brière et al. (2010), who neglected waves in their study of the morphodynamic evolution of the Kwinte Bank, did not find any significant recovery of the ridge during a period of 30 years.

Results furthermore demonstrate that extracting a large amount of sand (by creating deep pits) from a ridge initially destabilizes this ridge, i.e., the sand volume of the ridge declines in the first tens of years after extraction prior to its recovery in the subsequent time period (Fig. 13c). Destabilization of the ridge due to sand extraction is also observed on the Belgian shelf, where an annual decline of the volume of the Kwinte Bank (a tidal sand ridge of the Flemish banks, which has been subject to intense sand extraction since the 1970s) was reported by Norro et al. (2006). Note that direct volume losses due to extraction were excluded. Another indication of a loss of sand from the Kwinte Bank is the observed deepening of the sand pit that was created on this ridge, even after cessation of extraction activities in 2003 (Degrendele et al., 2010). The model outcomes suggest that, although the Kwinte Bank has been experiencing a decline of its sand volume, it probably would recover on longer time scales. Based on Eq. (5) and using the measured current velocities and sediment transport at the location of the sand pit (0.6 m s^{-1} and 5.3×10^{-5} $m^3\ s^{-1}\ m^{-1}$, respectively, Giardino et al., 2010), the recovery of the Kwinte Bank is estimated to be $t_r \sim 330$ years. However, the limited availability of sand on the Belgian shelf (Van Lancker et al., 2010) might delay or even prevent the recovery of this ridge.

4.4. Model limitations

The present depth-averaged model neglects the vertical structure of currents and suspended sediment concentrations. Hence, small-scale bedforms, such as sand waves, cannot form in this model (Hulscher, 1996). Sand waves, which are often present on top of tidal sand ridges, evolve on time scales of years to decades (Van Gerwen et al., 2018). Their evolution might significantly influence the sediment transport patterns and thus the morphodynamic evolution of the ridges (de Swart and Yuan, 2018, and reference therein). Resolving the vertical structure of currents and sediment concentrations is considered a topic of future research.

Furthermore, only one single tidal constituent (M_2) is considered in the tidal forcing, whereas other components are also present in the observed forcing (e.g. M_0, M_4, S_2). In particular, adding the M_0 and M_4 components are expected to increase the asymmetry of the tidal sand ridges, to enhance their migration and to reduce their heights (Roos et al., 2004). Furthermore, a constant wave forcing (constant wave height, period and direction) is assumed, whereas in reality this forcing is spatially and time varying.

A third assumption is that the water depth and the tidal forcings are constant during the simulation. However, tidal sand ridges evolve on the same time scale (decades to centuries) as sea-level rise (SLR) and changes in the background tidal current (Beets and van der Spek, 2000). Yuan and de Swart (2017) explored the effect of sea-level rise and related changes in tidal current on the long-term evolution of the tidal sand ridges. They found that in the case of an increasing mean sea level and the related decline in the flow velocity, ridges might become inactive and drown.

Another model limitation concerns the assumed weak interaction between the shelf and the nearshore zone by imposing a vanishing cross-shore flow at the shoreward boundary of the model domain, thereby neglecting advective sediment transport. This condition is motivated by the fact that these bed forms are trapped on continental shelves. However, significant sediment exchange might exist between the shelf and the nearshore zone (Schwab et al., 2013), with potential implications for the dynamics of the ridges and the stability of the coast. In particular, it would be interesting to investigate how the nearshore zone would be affected in the case of sand extractions and presence of

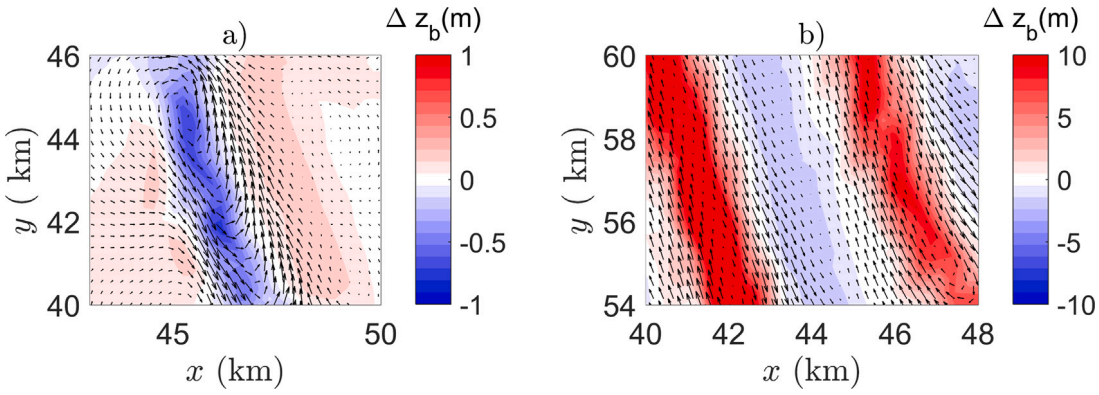

Fig. 12. (a–b) Residual flow field (arrows) at t = 550 yr, which are induced by the difference Δz_b (colours) between the bed levels of the cases with and without extraction ('SandpitDefault', panel a) and by the difference between the bed levels of the cases with and without an island ('IslandDefault', panel b). (For interpretation of the references to colour in this figure legend, the reader is referred to the web version of this article.)

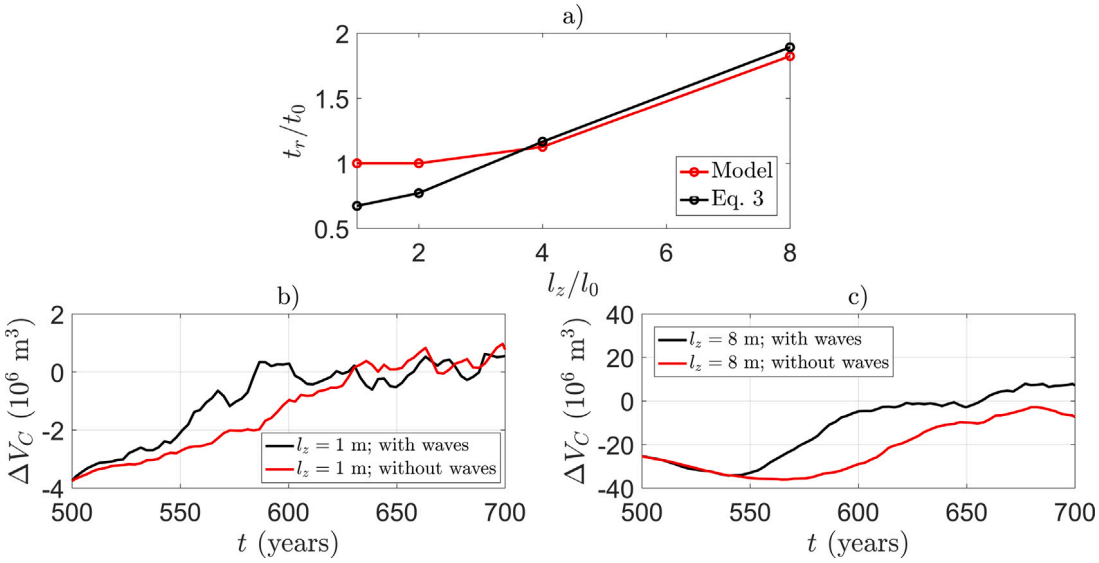

Fig. 13. (a) Modelled (red line) and estimated (using Eq. (5) in the main article, black line) recovery time scales t_r of the ridge crest for different pit depths l_z. Time scale t_r and depth l_z are scaled with their corresponding values in the case of the default sand extraction (t_0 = 87 yr and l_0 = 1 m, respectively). (b–c) Time evolution of the differences between the crest volumes (ΔV_C) of the cases with (black lines) and without (red lines) waves and for pit depths l_z = 1 m (b) and l_z = 8 m (c). (For interpretation of the references to colour in this figure legend, the reader is referred to the web version of this article.)

islands. Coupling of the present model with an existing model of the nearshore zone is currently a topic of research.

Another model limitation is that uniform grain size is assumed, while in reality variation in the grain size over tidal sand ridges is observed (Roos et al., 2007). Finally, the sea bed is assumed to provide an unlimited amount of sand, whereas in nature variations in the bed layer thickness exist. In particular, the recovery of sand ridges from sand extraction might be delayed or even prevented by a lack of sediment in the bed (Van Lancker et al., 2010).

4.5. Novelty of the model and its potential applications

The novelty of this model is that the morphodynamic evolution of tidal sand ridges and their response to interventions are studied in a more close-to-reality model setting compared with the previous studies. Specifically, among other things, a sophisticated wave model, a sloping shelf bottom and top-of-the-line formulations for bed load and suspended load transports were considered. The importance of these model aspects for the ridge dynamics is highlighted in the SI (Section S3). It turns out that the presence of waves enhances ridge growth and affect the spatial pattern of the ridges. On a flat shelf bathymetry ridge crests become higher compared with those on a sloping bottom. Suspended load transport causes mature ridges to form on centennial time scales, while they form on time scales of 10^3 years when this transport is neglected.

Furthermore, the advantage of the present model is that close-to-reality model settings can easily be applied, as they are built-in functionalities of the model. Moreover, this model can easily be adapted to study ridges at other locations, where for e.g. river discharge is important. This holds in particular for areas like the Yellow Sea and the East China Sea, where the continental shelves are receiving large amounts of sediments and fresh water from big rivers. Last but not least, the present model has built-in modules that allow a coupling to ecological models, with which possible implications of human interventions on the local ecology can be examined.

5. Conclusions

This study used a numerical model (coupled Delft3D-SWAN) to study the natural morphodynamic evolution of sand ridges and their response to interventions (sand extraction and construction of islands) in a more close-to-reality model setting compared with previous studies. Specifically, among other things, a sophisticated wave model, a

sloping shelf bottom and top-of-the-line formulations for bed load and suspended load transports were considered.

Model results show that mature ridges form on the shelf that resemble the observed tidal sand ridges. Results further demonstrate that ridges recover from sand extraction on decadal time scales. Sand needed for this recovery is provided by deepening of the troughs. Far offshore located sand ridges recover slower from sand extraction than onshore located ridges. Although deeper pits delay the recovery of the ridges, this recovery takes place at a more rapid pace than in the case of shallower pits. The presence of waves enhances the recovery of ridges. A ridge subjected to a too deep pit might loose sand in the first tens of years prior to its recovery on longer time scales. This initial loss of sand seems to agree with the observed decline of the sand volume of the Kwinte Bank, which has been subject to intense extractions for many decades.

Ridges in the vicinity of an island break into smaller scale bottom features, which have smaller orientation angles than those of the natural case. The island loses sand on a time scale of decades until it eventually disappears. This sand loss is deposited on the crests and in the troughs. Implementing different island configurations does not qualitatively change model results. The main quantitative differences are that crests undergo more sedimentation in the case of either increasing the offshore distance or number of islands and undergo less sedimentation for larger longshore spacings between islands.

Finally, model results show that a local bathymetric disturbance on the shelf (sand pit, island) evolves into large-scale elongated and cyclonically oriented bedforms, which increasingly cover the shelf with time. Thus, introducing a local disturbance eventually affects the sand volumes of other ridges on the shelf as well.

Declaration of competing interest

The authors declare that they have no known competing financial interests or personal relationships that could have appeared to influence the work reported in this paper.

Appendix A. Supplementary data

Supplementary material related to this article can be found online at https://doi.org/10.1016/j.csr.2020.104195.

References

Atalah, J., Fitch, J., Coughlan, J., Chopelet, J., Coscia, I., Farrell, E., 2013. Diversity of demersal and megafaunal assemblages inhabiting sandbanks of the Irish Sea. Mar. Biodiversity 43, 121–132.

Baeye, M., Fettweis, M., Voulgaris, G., Van Lancker, V., 2011. Sediment mobility in response to tidal and wind-driven flows along the Belgian shelf, southern North Sea. Ocean Dyn. 61, 611–622. http://dx.doi.org/10.1007/s10236-010-0370-7.

Battjes, J.A., Janssen, J.P.F.M., 1978. Energy loss and set-up due to breaking of random waves. In: Coastal Engineering Proceedings 1978. pp. 569–587. http://dx.doi.org/10.1061/9780872621909.034.

Beets, D.J., van der Spek, A.J.F., 2000. The holocene evolution of the barrier and the back-barrier basins of Belgium and the netherlands as a function of late weichselian morphology, relative sea-level rise and sediment supply. Netherlands J. Geosci. Geol. Mijnbouw 79, 3–16. http://dx.doi.org/10.1017/S0016774600021533.

Blondeaux, P., 2001. Mechanics of coastal forms. Annu. Rev. Fluid Mech. 33, 339–370.

Booij, N., Holthuijsen, L., Ris, R., 1996. The SWAN wave model for shallow water. In: Coastal Engineering Proceedings 1996. pp. 668–676. http://dx.doi.org/10.1061/9780784402429.053.

Brière, C., Roos, P.C., Garel, E., Hulscher, S., 2010. Modelling the morphodynamics of the Kwinte bank, subject to sand extraction. J. Coast. Res. SI 51, 117–126.

Caston, V.N.D., 1972. Linear sand banks in the southern North Sea. Sedimentology 18, 63–78. http://dx.doi.org/10.1111/j.1365-3091.1972.tb00003.x.

Davis, R.A., Klay, J., Jewell, P., 1993. Sedimentology and stratigraphy of tidal sand ridges southwest Florida inner shelf. J. Sediment. Res. 63, 91–104.

De Clercq, M., Chademenos, V., Van Lancker, V., Missiaen, T., 2016. A high-resolution DEM for the Top-Palaeogene surface of the Belgian Continental Shelf. J. Maps 12, 1047–1054.

De Maerschalck, B., van der Werf, J., Kolokythas, G.K., Quataert, E., van Oyen, T., Vroom, J., Dijkstra, J., Wang, Z.B., Vanlede, J., Verwaest, T., et al., 2017. Modellering Belgische kustzone en Scheldemonding: deelrapport 2. Morfologische analyse scenario's Vlaamse Baaien.

de Swart, H.E., Yuan, B., 2018. Dynamics of offshore tidal sand ridges, a review. Environ. Fluid Mech. 1–25.

Degrendele, K., Roche, M., Schotte, P., Va. Lancker, V., Bellec, V.K., Bonne, W., 2010. Morphological evolution of the kwinte bank central depression before and after the cessation of aggregate extraction. J. Coast. Res. SI 51, 77–86.

Deltares, 2019. User Manual Delft3D-FLow: Simulation of Multi-Dimensional Hydrodynamic Flows and Transport Phenomena, Including Sediments. Technical Report. Version 3.15, SNV Revision: 60015, Delft, the Netherlands.

Dodd, N., Blondeaux, P., Calvete, D., De Swart, H.E., Falqués, A., Hulscher, S.J.M.H., Rózyński, G., Vittori, G., 2003. Understanding coastal morphodynamics using stability methods. J. Coast. Res. 33, 849–865.

Dyer, K.R., Huntley, D.A., 1999. The origin, classification and modelling of sand banks and ridges. Cont. Shelf Res. 19, 1285–1330.

Giardino, A., Van den Eynde, D., Monbaliu, J., 2010. Wave effects on the morphodynamic evolution of an offshore sand bank. J. Coast. Res. 51, 127–140.

Hasselmann, K., Barnett, T., Bouws, E., Carlson, H., Cartwright, D., Enke, K., Ewing, J., Gienapp, H., Hasselmann, D., Kruseman, P., 1973. Measurements of wind-wave growth and swell decay during the Joint North Sea Wave Project (JONSWAP). Deutsche Hydrogr. Z. 12, 1–95.

Hulscher, S.J.M.H., 1996. Tidal-induced large-scale regular bed form patterns in a three-dimensional shallow water model. J. Geophys. Res. Oceans 101, 20727–20744.

Huthnance, J., 1982a. On the formation of sand banks of finite extent. Estuar. Coast. Shelf Sci. 15, 277–299.

Huthnance, J.M., 1982b. On one mechanism forming linear sand banks. Estuar. Coast. Shelf Sci. 14, 79–99.

Jiabi, D., Wang, Y., 2014. Evolution simulation of radial sand ridges in the southern Yellow Sea. J. Nanjing Univ. Nat. Sci. 50, http://dx.doi.org/10.13232/j.cnki.jnju.2014.05.012.

Kenyon, N.H., Belderson, R.H., Stride, A.H., Johnson, M.A., 1981. Offshore tidal sand banks as indicators of net sand transport and as potential deposits. Holocene Mar. Sediment. North Sea Basin 5, 257–268.

Komen, G.J., Hasselmann, K., 1984. On the existence of a fully developed wind-sea spectrum. J. Phys. Oceanogr. 14, 1271–1285.

Lesser, G.R., Roelvink, J.A., Van Kester, J.A.T.M., Stelling, G.S., 2004. Development and validation of a three-dimensional morphological model. Coast. Eng. 51, 883–915. http://dx.doi.org/10.1016/j.coastaleng.2004.07.014.

Liu, Z., Berné, S., Saito, Y., Yu, H., Trentesaux, A., Uehara, K., Yin, P., Liu, J.P., Li, C., Hu, G., et al., 2007. Internal architecture and mobility of tidal sand ridges in the East China Sea. Cont. Shelf Res. 27, 1820–1834.

Norro, A., Pichot, G., Pison, V., Ozer, J., 2006. A bi-dimensional approach to assessing the volumetric evolution of an exploited sandbank. ICES J. Mar. Sci. 63, 176–186. http://dx.doi.org/10.1016/j.icesjms.2005.08.006.

Off, T., 1963. Rhythmic linear sand bodies caused by tidal currents. AAPG Bull. 47, 324–341.

Roelvink, J.A., 2006. Coastal morphodynamic evolution techniques. Coast. Eng. 53, 277–287. http://dx.doi.org/10.1016/j.coastaleng.2005.10.015.

Roelvink, J.A., Walstra, D.J., 2004. Keeping it simple by using complex models. Adv. Hydro-Sci. Eng. 6, 1–11.

Roos, P.C., Hulscher, S.J., 2007. Nonlinear modeling of tidal sandbanks: wavelength evolution and sand extraction. In: Coastal Engineering 2006: (in 5 Volumes). World Scientific, pp. 2761–2771.

Roos, P.C., Hulscher, S.J.M.H., Knaapen, M.A.F., Van Damme, R.M.J., 2004. The cross-sectional shape of tidal sandbanks: Modeling and observations. J. Geophys. Res. Earth Surf. 109.

Roos, P.C., Hulscher, S.J.M.H., de Vriend, H.J., 2008. Modelling the morphodynamic impact of offshore sandpit geometries. Coast. Eng. 55, 704–715.

Roos, P.C., Wemmenhove, R., Hulscher, S.J., Hoeijmakers, H.W., Kruyt, N., 2007. Modeling the effect of nonuniform sediment on the dynamics of offshore tidal sandbanks. J. Geophys. Res. Earth Surf. 112.

Ryan, W.B.F., Carbotte, S.M., Coplan, J.O., O'Hara, S., Melkonian, A., Arko, R., Weissel, R.A., Ferrini, V., Goodwillie, A., Nitsche, F., Bonczkowski, J., Zemsky, R., 2009. Global multi-resolution topography synthesis. Geochem. Geophys. Geosyst. 10, http://dx.doi.org/10.1029/2008GC002332.

Schwab, W.C., Baldwin, W.E., Hapke, C.J., Lentz, E.E., Gayes, P.T., Denny, J.F., List, J.H., Warner, J.C., 2013. Geologic evidence for onshore sediment transport from the inner continental shelf: Fire Island, New York. J. Coast. Res. 29, 526–544. http://dx.doi.org/10.2112/JCOASTRES-D-12-00160.1.

Spencer, T., Brooks, S.M., Evans, B.R., Tempest, J.A., Möller, I., 2015. Southern North Sea storm surge event of 5 December 2013: water levels, waves and coastal impacts. Earth-Sci. Rev. 146, 120–145.

Tao, J., Wang, Z.B., Zhou, Z., Xu, F., Zhang, C., Stive, M.J., 2019. A morphodynamic modeling study on the formation of the large-scale radial sand ridges in the southern Yellow Sea. J. Geophys. Res. Earth Surf. http://dx.doi.org/10.1029/2018JF004866.

van Dijk, T.A.G.P., van Dalfsen, J.A., Van Lancker, V., van Overmeeren, R.A., van Heteren, S., Doornenbal, P.J., 2012. Benthic habitat variations over tidal ridges, North Sea, the Netherlands. In: Seafloor Geomorphology As Benthic Habitat. Elsevier, pp. 241–249.

Van Gerwen, W., Borsje, B.W., Damveld, J.H., Hulscher, S.J.M.H., 2018. Modelling the effect of suspended load transport and tidal asymmetry on the equilibrium tidal sand wave height. Coast. Eng. 136, 56–64. http://dx.doi.org/10.1016/j.coastaleng.2018.01.006.

Van Lancker, V.R.M., Bonne, W.M.I., Garel, E., Degrendele, K., Roche, M., Van den Eynde, D., Bellec, V.K., Brière, C., Collins, M.B., Velegrakis, A.F., 2010. Recommendations for the sustainable exploitation of tidal sandbanks. J. Coast. Res. SI 51, 151–164.

Van Rijn, L.C., 1993. Principles of Sediment Transport in Rivers, Estuaries and Coastal Seas. Aqua publications Amsterdam.

van Veelen, T.J., Roos, P.C., Hulscher, S.J.M.H., 2018. Process-based modelling of bank-breaking mechanisms of tidal sandbanks. Cont. Shelf Res. 167, 139–152. http://dx.doi.org/10.1016/j.csr.2018.04.007.

Verwaest, T., Doorme, S., Verelst, K., Trouw, K., 2011. The wave climate in the Belgian coastal zone. In: Proceedings 9th International Conference LITTORAL: A Changing Coast: Challenge for the Environmental Policies, Venice, Italy, pp. 1–8.

Yuan, B., de Swart, H.E., 2017. Effect of sea level rise and tidal current variation on the long-term evolution of offshore tidal sand ridges. Mar. Geol. 390, 199–213.